Relaxation Control of Open Quantum Systems

Nicolò Beato* and Gianluca Teza†
Max Planck Institute for the Physics of Complex Systems, Nöthnitzer Straße 38, 01187 Dresden, Germany

(Received 30 July 2025; revised 10 November 2025; accepted 8 January 2026; published 18 February 2026)

A fundamental problem in experiments with open quantum systems is to ensure steady-state convergence within a given operational time window. Here, we devise a general state preparation recipe to control relaxation timescales and achieve steady-state convergence within experimental run times. We do so by constructing a unitary operation that cancels multiple relaxation modes. We provide an example in a few-body interacting system (long-range qubit chain), taking into account limitations of experimentally accessible unitary operations in quantum simulators.

DOI: 10.1103/4frd-ck2z

Preparing a system in a desired equilibrium configuration often requires exploring paths that are far from equilibrium. In the presence of dissipation, the system evolves toward a steady state with a relaxation timescale set by its intrinsic properties, initial conditions, and environment [1]. In the context of quantum simulation on noisy intermediate-scale quantum devices [2], one has to face the challenge of physical and experimental constraints limiting the overall time for a reliable observation of the dynamics [3–9]. To prepare the system in a desired physical state, it is therefore essential to design protocols that accelerate relaxation, ensuring convergence within the operating time window [10–12].

Outside equilibrium, recent advances in tackling this fundamental problem set their roots in the Mpemba effect, a phenomenon originally related to the possibility of freezing water faster by starting from an initially hotter temperature [13,14]. After the characterization of the Mpemba effect within a Markovian framework [15,16], several strategies were developed to accelerate the relaxation timescale in dissipative systems in classical [17–20] and quantum [21–25] settings. The idea behind these strategies is to reduce the overlap of the initial condition with the slowest relaxation mode of the dynamics, related to the second dominant eigenvalue of the evolution operator [15,26]. This idea has been experimentally validated in single-particle systems, including colloidal setups [27–29] and trapped ions quantum simulators [30,31], leading to the observation of novel anomalous relaxation phenomena in classical [20,32–36] and quantum systems, both open [37–40] and closed [41–43].

In few- and many-body interacting systems, this simplified picture can easily break down, as the gap between the slowest mode and the following ones typically vanishes or is comparatively small with respect to their values [10,44]. This is particularly fundamental for systems possessing multiple steady states, which can host phenomenology relevant for quantum technologies (e.g., dark states, unitarily evolving subspace, enhanced quantum transport [45–48]) that remain inaccessible when the relaxation does not occur within the experimental time window. Additionally, the complementary problem of extending the relaxation lifetime is also of fundamental relevance (e.g., to increase classification capabilities of quantum neural networks [49]), but remains unaddressed to this day.

In this Letter, we introduce a general recipe for eliminating multiple relaxation modes in an open quantum system via a unitary operation, which enables the tuning of relaxation timescales without requiring any active control during the evolution. The concurrent suppression of multiple modes unlocks a variety of applications, including, for instance, relaxation speedups even in the presence of dense, slow-decaying modes. In our strategy, we first identify the relaxation modes that need to be suppressed to obtain the desired speedup in the relaxation dynamics and project the initial state ρ_0 outside of their associated subspace. As this operation does not immediately yield a physical state (i.e., density matrix), we then reconstruct a state $\rho_\perp$ preserving the vanishing overlap with the undesired relaxation modes within desired precision. Finally, we build a unitary operation U such that $\rho_\perp = U\rho_0 U^\dagger$. We provide an example in a few-body interacting system (long-range qubit chain), where we investigate the effect of experimental limitations in the allowed unitary operations encountered in quantum simulators.

Setup—The dynamics of Markovian open quantum systems is described by the Gorini-Kossakowski-Sudarshan-Lindblad equation [50–60], which regulates the evolution of

*Contact author: nbeato@pks.mpg.de
†Contact author: teza@pks.mpg.de

Published by the American Physical Society under the terms of the Creative Commons Attribution 4.0 International license. Further distribution of this work must maintain attribution to the author(s) and the published article's title, journal citation, and DOI. Open access publication funded by the Max Planck Society.

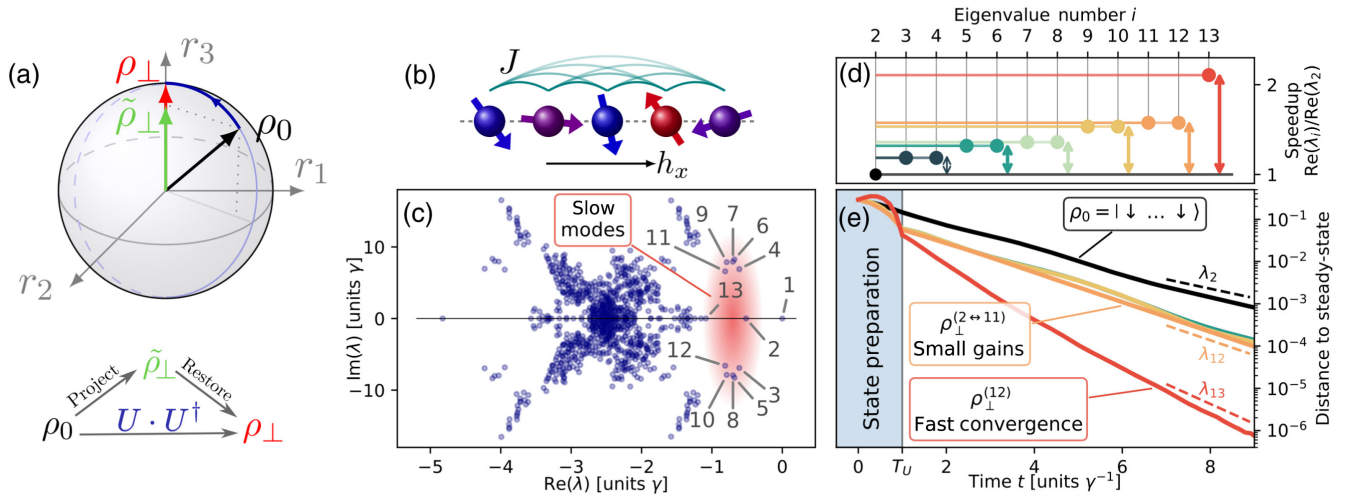


FIG. 1. Schematics representing the selective suppression of eigenmodes of the Liouvillian operator [cf. Eq. (2)] and exponential speedup of the relaxation. (a) A unitary rotation allows to cancel the projection of an arbitrary initial state ρ_0 along undesired decaying modes, which is here illustrated as the rotation of a three-dimensional vector ρ_0 into the vector $\rho_\perp$, perpendicular to the undesired directions r_1, r_2. (c) Spectrum of the Liouvillian for the long-range Ising chain sketched in panel (b) and defined in Eqs. (9) and (10) ($N = 5, h_x = 1, J = 1.25, \alpha = 0.5$, and $\gamma = 1$). While the relaxation timescale $\tau = |\mathrm{Re}\lambda_2^{-1}|$ is regulated by the second dominant eigenvalue, eigenvalues $\lambda_3, \ldots, \lambda_{12}$ have comparable real parts (red shaded area). In this scenario, suppressing the second eigenmode would not provide any practical advantage. (d) Speedups [in terms of $\mathrm{Re}(\lambda_i)/\mathrm{Re}(\lambda_2)$] achievable through multimode suppression. Notice the considerable gap dividing the 12th and 13th eigenvalues in the example. (e) Comparison of the different relaxations to the steady state ρ_∞ obtained by applying our recipe to the fully down-polarized initial state $|\downarrow, \ldots, \downarrow\rangle$ [cf. Eq. (11)]. We selectively suppress the projection of the initial density matrix ρ_0 along the first $n = 2, 3, \ldots, 12$ slowest decaying modes. While cancellation up to the 11th mode does not sensibly change the relaxation timescale, simultaneous suppression of the first 12 modes provides a faster convergence, $\mathrm{Re}(\lambda_{13})/\mathrm{Re}(\lambda_2) \approx 2$.

the density matrix $\rho(t)$ in terms of the master equation $\dot{\rho}(t) = \mathcal{L}[\rho(t)]$,

$$\mathcal{L}[\rho] = -i[H,\rho] + \sum_{i=1}^{N_J}\left(L_i\rho L_i^\dagger - \frac{1}{2}\{L_i^\dagger L_i, \rho\}\right). \quad (1)$$

The Liouville superoperator $\mathcal{L}$ is the generator of a completely positive trace-preserving map, H is the Hamiltonian of the system, and $\{L_i\}_1^{N_J}$ are $N_J \in \mathbb{N}$ jump operators accounting for incoherent and dissipative effects.

For a diagonalizable Liouvillian, one can find the right and left (eigen)modes $\{r_k\}, \{\ell_k\}$ and eigenvalues $\{\lambda_k\}$, labeled by the index k and satisfying [61]

$$\mathcal{L}[r_k] = \lambda_k r_k, \qquad \mathcal{L}^\dagger[\ell_k] = \lambda_k^* \ell_k. \quad (2)$$

In general, λ_k is complex valued [see e.g. Fig. 1(c)] and $r_k \neq \ell_k$ can be chosen to satisfy the biorthonormality relation $\mathrm{Tr}(\ell_k^\dagger r_m) = \delta_{km}$ [60,62–64]. In the case of real eigenvalue, $\lambda_k \in \mathbb{R}$, the associated modes r_k, ℓ_k are Hermitian, $r_k = r_k^\dagger$, $\ell_k = \ell_k^\dagger$. Similar to the unitary case, the nonunitary evolution operator generated by the Lindblad map can be explicitly written using its spectral decomposition as

$$\exp(t\mathcal{L})[\rho_0] = \sum_{k=1}^{d^2} \mathrm{Tr}\left(\ell_k^\dagger \rho_0\right) e^{t\lambda_k} r_k, \quad (3)$$

with d the Hilbert space dimension. The complete positivity of $\mathcal{L}$ implies a nonpositive real part of the spectrum, allowing us to sort the eigenvalues according to $\mathrm{Re}(\lambda_i) \geq \mathrm{Re}(\lambda_{i+1})$, $i = 1, \ldots, d^2 - 1$. For bounded systems, Evans' theorem guarantees the existence of at least one steady state (or nonequilibrium steady state), associated with the vanishing eigenvalue, $\lambda_1 = 0$ [65,66]. Open quantum systems can generally exhibit multiple steady states [45,47,63,67,68] associated to the zero eigenvalue, and/or modes associated with purely imaginary eigenvalues, named "stationary coherences" [62,69–72]. In the following, we indicate with d_s the number of eigenvalues with vanishing real part, and collectively refer to the associated modes as "nondecaying." The projection of ρ_0 lying on the subspace of decaying modes, $\{r_k\}_{k=d_s+1}^{d^2}$, is exponentially suppressed by the coefficients $\{e^{t\mathrm{Re}(\lambda_k)}\}_{k=d_s+1}^{d^2}$. At sufficiently large times the slowest decaying modes dominate the dynamics, $\rho(t) \sim \rho_\infty(t) + e^{-|\mathrm{Re}(\lambda_{d_s+1})|t} r_{d_s+1}$, and the smallest decay rate $\tau^{-1} = |\mathrm{Re}(\lambda_{d_s+1})|$ sets the system's relaxation timescale.

Speedup of relaxation—The basic idea behind the realization of a Mpemba effect in dissipative systems is

to find an initial condition orthogonal to the slowest decaying mode [15,21], which, in the case of a unique steady state, is set by the real part of the second dominant eigenvalue of the evolution operator λ_2. However, a rather common scenario is that of a small (or missing) gap separating λ_3 from λ_2 [55], which completely undermines this strategy and its relevance for experimental contexts. We overcome these limitations by introducing a recipe to suppress, through a unitary operation U, the overlap $\mathrm{Tr}(\ell_a^\dagger U\rho_0 U^\dagger)$ of the initial state ρ_0, with multiple modes $\ell_a \in \mathcal{A} \subset \{\ell_k\}_{k=1}^{d^2}$, associated with real or (pairs of) complex eigenvalues. Theoretical restrictions and experimental challenges of our recipe are tied to physically relevant constraints and will be discussed in what follows.

Consider a finite-dimensional open quantum system, whose evolution is described by the Gorini-Kossakowski-Sudarshan-Lindblad equation [Eq. (1)]. We now construct a unitary operator U such that $\rho_\perp = U\rho_0 U^\dagger$ satisfies $\mathrm{Tr}(\ell_a \rho_\perp) < \epsilon,\ \forall\ \ell_a \in \mathcal{A}$, for a positive arbitrary small ϵ. We structure the procedure leading to the construction of the operator U in four main steps, which we outline in detail below and illustrate in Fig. 1(a) with a sketch.

Step 1. Orthogonal projection: First, we identify the undesired Lindblad modes $\ell_a \in \mathcal{A}$ and project the initial state ρ_0 outside of the associated subspace. To this end, we expand the initial state ρ_0 into the Lindblad eigenbasis [73],

$$\rho_0 = \sum_{k=1}^{d^2} c_k r_k, \qquad c_k = \mathrm{Tr}\left(\ell_k^\dagger \rho_0\right). \tag{4}$$

Then, we construct the operator $\tilde{\rho}_\perp$,

$$\rho_0 \mapsto \tilde{\rho}_\perp = \sum_{k=1}^{d^2} \tilde{c}_k r_k, \quad c_k \mapsto \tilde{c}_k = \begin{cases} 0 & k:\ \ell_k \in \mathcal{A} \\ c_k & k:\ \ell_k \notin \mathcal{A} \end{cases}, \tag{5}$$

where the coefficients associated with the undesired components are set to zero. This procedure projects ρ_0 out of the subspace associated with modes $\ell_a \in \mathcal{A}$ but does not generally yield a density matrix. First, $\tilde{\rho}_\perp$ is hermitian, $\tilde{\rho}_\perp = \tilde{\rho}_\perp^\dagger$, if and only if the chosen set $\mathcal{A}$ is stable under Hermitian conjugation, $\mathcal{A} = \mathcal{A}^\dagger$ [74]. Here and in the remainder of this Letter, we will make this assumption. Second, in general, the operator $\tilde{\rho}_\perp$ is not a density matrix and does not possess the same spectrum as ρ_0; therefore, no unitary transformation U satisfying $\tilde{\rho}_\perp = U\rho_0 U^\dagger$ exists. This problem is fixed in the second and third steps of the recipe, where we construct the density matrix $\rho_\perp$, which possesses the same spectrum as the initial state ρ_0 and is orthogonal to the modes $\ell_a \in \mathcal{A}$ up to precision ϵ.

Step 2. Trace and purity restoration: We restore the trace and purity of ρ_0 by rescaling the coefficients of $\tilde{\rho}_\perp$. We introduce two independent real parameters, $\alpha_s, \alpha \in \mathbb{R}$, and separately rescale the coefficients of the nondecaying and decaying modes,

$$\tilde{\rho}_\perp \mapsto \bar{\rho}_\perp = \sum_{k=1}^{d^2} \bar{c}_k r_k, \quad \tilde{c}_k \mapsto \bar{c}_k = \begin{cases} \alpha_s \tilde{c}_k & k \le d_s \\ \alpha \tilde{c}_k & k > d_s \end{cases}. \tag{6}$$

In [63], we give the expressions relating α_s, α to the initial state and projected operator $\rho_0, \tilde{\rho}_\perp$, and discuss sufficient conditions for the existence of the real coefficient α. In particular, we prove that α always exists in two important cases, namely when (i) only decaying modes [$\mathrm{Re}(\lambda_k) < 0$] are suppressed or (ii) the initial state ρ_0 is pure. Overall, the second step yields the operator $\bar{\rho}_\perp$, orthogonal to the Liouvillian left eigenmodes $\ell_a \in \mathcal{A}$ by construction, and satisfying the conservation of trace and purity,

$$1 = \mathrm{Tr}(\bar{\rho}_\perp) = \mathrm{Tr}(\rho_0), \qquad \mathrm{Tr}(\bar{\rho}_\perp^2) = \mathrm{Tr}(\rho_0^2). \tag{7}$$

Step 3. Spectrum matching: We enforce the equality of the spectrum between the initial and transformed states, $\rho_0, \rho_\perp$. We diagonalize the initial density matrix ρ_0 and the operator $\bar{\rho}_\perp$ [75],

$$\rho_0 = U_1 D_1 U_1^\dagger \qquad \bar{\rho}_\perp = U_2 D_2 U_2^\dagger, \tag{8}$$

and construct the density matrix

$$\rho'_\perp = U_2 D_1 U_2^\dagger.$$

By construction, the state $\rho'_\perp$ possesses the same spectrum as ρ_0. However, when $D_2 \neq D_1$, $\rho'_\perp$ is not exactly orthogonal to the set $\mathcal{A}$. To this end, we therefore iterate the three steps of the recipe until numerical convergence is achieved (see Ref. [63] for a discussion of convergence properties). In this way, upon convergence of the iterative procedure within tolerance ϵ, we obtain a well-defined density matrix $\rho_\perp$, which is orthogonal to the Liouvillian modes $\mathcal{A}$ to precision ϵ [76].

Step 4. Unitary Transformation: Lastly, we find a unitary operator U generating the transformation $\rho_\perp = U\rho_0 U^\dagger$. As we constructed the density matrix $\rho_\perp$ with the same spectrum as ρ_0, there always exists a theoretically available unitary transformation U connecting the two physical states [63]. In experiments, one faces the challenge of using a limited set of generators, e.g., single-qubit operators. This is a *state-preparation problem*, to be solved using the toolbox of optimal quantum control theory [77,78]; the existence of a solution depends on the particular set of generators allowed by the experimental apparatus [79,80]. For this reason, in what follows, we restrict the discussion to a specific open quantum system and show how our recipe works in practice.

Applications—We demonstrate the capability of our recipe by applying it to a long-range interacting N-qubit chain, accessible experimentally in current trapped ions and Rydberg atom quantum simulators [3–9]. The coherent

evolution is generated by the Hamiltonian

$$H = h_x \sum_{i=1}^{N} \sigma_i^x + J \sum_{i<j}^{N} \frac{\sigma_i^z \sigma_j^z}{|i-j|^\alpha}, \tag{9}$$

where $\sigma_i^a, a = x, y, z$ are Pauli matrices, h_x sets the intensity of the external x-magnetic field, and J, α control the strength and range, respectively, of the spin-spin interaction. The dissipative dynamics is generated by the jump operators,

$$L_i = \sqrt{\gamma}\sigma_i^- \qquad \sigma_i^- = (\sigma_i^x - i\sigma_i^y)/2, \tag{10}$$

describing a spontaneous decay process from the state $|\uparrow_i\rangle$ to $|\downarrow_i\rangle$ with rate γ. This model has a unique steady state, so we have $d_s = 1$ [cf. Fig. 1(c)]. In the following, we use the completely down-polarized initial state $\rho_0 = |\downarrow, \ldots, \downarrow\rangle$.

As a first example, we engineer an exponential speedup of the relaxation toward the steady state by suppressing components of ρ_0 along the first slowest-decaying modes $\mathcal{A}_\perp^{(n)} = \{\ell_a\}_{a=2}^{n}$, for $2 \le n \le 12$. In Fig. 1(c), we show the evolution of the trace norm [81],

$$d(\rho_1, \rho_2) = (1/2)\mathrm{Tr}\sqrt{|\rho_1 - \rho_2|^2}, \tag{11}$$

of the initial and transformed states, $\rho, \rho_\perp^{(n)}$ (black and colored curves, respectively) to the steady state ρ_∞. The number of suppressed components n controls the decay rate and exponentially accelerates the convergence to the steady state. In this example, we observe how eliminating the first ten slowest-decaying modes ($n \le 11$) does not provide any substantial change in the slope of the curves of $\rho_\perp^{(n)}(t)$ [Fig. 1(e)]. This is due to the presence of a dense cluster of slow eigenvalues $\{\lambda_k\}_{i=2}^{12}$ in the spectrum of the Liouvillian operator [Fig. 1(c)]: only the simultaneous suppression of all such modes yields a substantial speedup.

In Fig. 2, we investigate the effectiveness of the exponential speedup recipe for different parameters of the Liouvillian. We vary $\alpha = 0.5, 1.0, 2.0$, $h_x, J \in [0.25, 4.0]$,

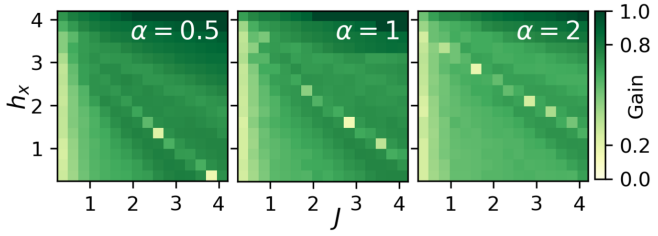


FIG. 2. Speedup of the relaxation dynamics for different parameters α, h_x, J of the Liouvillian in Eqs. (9) and (10). The three figures display the relative time gain achieved by the transformed state $\rho_\perp$, as compared to the original state ρ_0 [cf. Eq. (12)]. The time gain is generally a significant fraction of the original time (i.e., 50%), except for few isolated cases where the projection of the original state ρ_0 on the slowest Liouvillian eigenmodes already happens to be small.

and show the relative time gain achieved after suppressing up to the first 20 decaying Liouvillian modes. In particular, we consider the times $T, T_\perp$ required by the trace norm [cf. Eq. (11)] between $\rho_0(t), \rho_\perp(t)$, and ρ_∞ to reach the experimentally motivated threshold $D_{\min} = 10^{-3}$ and compute the relative time gain [82],

$$\mathrm{Gain} = 1 - T_\perp/T. \tag{12}$$

The results confirm the method's robustness and effectiveness across a wide parameter range. Indeed, the few cases where the recipe does not achieve a considerable gain (i.e., < 0.1) are due to the exceptionally small components of the original initial state ρ_0 onto the suppressed eigenmodes, $\ell_a \in \mathcal{A}$; in this rare situation, the relaxation timescale of ρ_0 is already fast compared to the modes we suppress.

A complementary application of our recipe is that of *extending* the lifetime of the relaxation dynamics. In the End Matter, we show how we can suppress the projection of the initial state ρ_0 on all except the slowest-decaying mode(s) $\{\ell_2\}$ (or $\{\ell_2, \ell_2^*\}$ in case $\lambda_2 = \lambda_3^*$) to increase the time needed for relaxation. In this case, the relaxation occurring with timescale $\tau = |\mathrm{Re}\lambda_2^{-1}|$ is not exponentially slower, but still retains a relative gain in the steady-state distance (compared to ρ_0) that is persistently maintained at long evolution time.

Speedup with local operations—In experiments, one must construct the unitary operation transforming the state ρ_0 into $\rho_\perp$ using only experimentally accessible operations [79,83]. We therefore investigate the practical utility of our recipe in trying to approximate the target states $\rho_\perp^{(n)}$ with the unitary operator [84]

$$U(\theta, \phi) = \bigotimes_{i=1}^{N} U_i(\theta, \phi)$$
$$U_i(\theta, \phi) = \exp(i\theta\sigma_i^z/2)\exp(i\phi\sigma_i^y/2). \tag{13}$$

Having only single-qubit operations, the unitary $U(\theta, \phi)$ is experimentally accessible in modern quantum devices [85–87] [88]. In particular, $U(\theta, \phi)$ uniformly rotates the qubits of the chain by the angles θ, ϕ (the only two parameters of the ansatz), along the axis σ_y, σ_z, respectively. This operation amounts to an arbitrary reorientation of each qubit by the same angles in the Bloch sphere. We optimize the parameters (θ, ϕ) to minimize the infidelity between $\rho_\perp$ and $\check{\rho}_\perp = U(\theta, \phi)\rho_0 U^\dagger(\theta, \phi)$.

In Fig. 3, we illustrate the steady-state convergence obtained preparing the system in the experimentally accessible state $\check{\rho}_\perp$. Despite experimental limitations, the recipe consistently yields a speedup in the steady-state convergence that progressively increases with the number n of suppressed modes. For comparison, we also report the convergence of the state $\rho_\perp^{(12)}$ prepared with the geodesic unitary [63]: a mismatch in the relaxation slope is to be expected, due to the exponential precision (in evolution

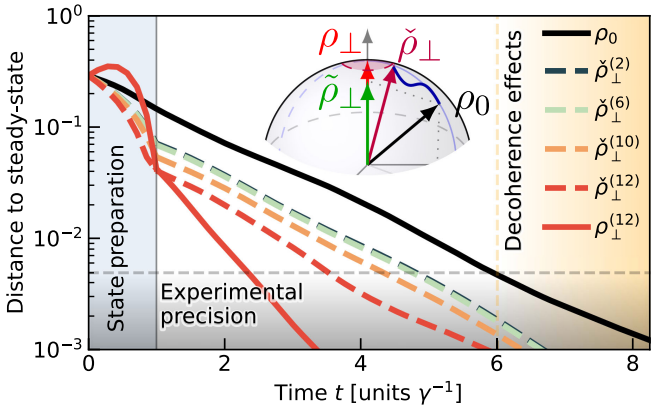


FIG. 3. Speedup of the relaxation dynamics toward the steady state, obtained through the experimentally accessible unitary transformations in Eq. (13), in the open quantum Ising chain in Eqs. (9) and (10) ($N = 5, h_x = 1, J = 1.25, \alpha = 0.5$, and $\gamma = 1$). The plot shows the distance to the steady state ρ_∞ of the initial state ρ_0 and the transformed states, $\check{\rho}_\perp^{(n)}$, obtained with the experimentally accessible unitary [black and dashed curves, respectively; cf. Eq. (11)]. For reference, we also plot the evolution of $\rho_\perp^{(12)}$ from Fig. 1(d), obtained with the geodesic unitary (solid red curve) [63]. Despite experimental limitations, the recipe produces a speedup in the steady-state convergence that progressively increases with the number n of suppressed modes.

time t) required in the unitary transformation for the suppression of the coefficients c_k. Nonetheless, the substantial gain in the steady-state distance (compared to ρ_0) provided by the preparation stage and the first phases of the relaxation is preserved throughout the entire relaxation process. In particular, the imperfections in the preparations set a timescale $|\lambda_2^{-1}|$ for all the curves, as in the "weak" version of the Mpemba effect [14,16].

More importantly, quantum experiments have a finite operational time window $T_{\max}$ and measurement sensitivity $D_{\min}$. As a reference, typical values for neutral-atom simulators lie on the order of 10 μs for the former and between 0.1% and 1% for the latter [6,7,89,90]. In Fig. 3, we highlight the experimentally inaccessible regimes with the (vertical) orange $T \gtrsim T_{\max}$ and (horizontal) gray $D \lesssim D_{\min}$ shaded regions; we notice that the transformed state $\check{\rho}_\perp^{(12)}$ reaches a threshold of distance $D_{\min} \in [10^{-2}, 10^{-3}]$ significantly earlier than $\check{\rho}_\perp^{(2-10)}$. This underlines how the unitary transformations, from an experimental and practical perspective, shall not necessarily reach unit fidelity in the preparation of the state $\rho_\perp$.

Discussion—Our method enables precise control over the relaxation dynamics of an open quantum system by selectively suppressing specific eigenmodes of the Liouvillian. While we proved its utility focusing on the speedup and slowdown of steady-state convergence, our recipe allows targeting an *arbitrary* set of eigenmodes, providing straightforward applications beyond the scenarios we presented. Additionally, our method also works in the presence of steady-state degeneracies, making it a powerful tool for the manipulation of the dissipative dynamics in systems with nontrivial spectral structure [62]. Examples include systems possessing degenerate steady states and/or a unitarily evolving subspace [47,48,91,92] and driven-dissipative systems [93–95]. Although the algorithm has already delivered excellent results in the systems we analyzed (cf. Fig. 2), advanced update methods could improve the algorithm's convergence and accuracy [96–98]. Lastly, preservation of the initial state's spectrum corresponds to a polynomial constraint satisfaction problem [99–103], supporting a quest toward exact solutions [104].

Acknowledgments—The authors gratefully acknowledge the late Professor Vittorio Gorini for providing advice and useful remarks in the final stages of this project, as well as Federico Balducci, Marin Bukov, Sergio Cacciatori, Francesco Campaioli, Mattia Moroder, and Ana Silva for discussions and feedback. The authors acknowledge support from the Max Planck Society. Numerical simulations were performed on the MPIPKS HPC cluster.

Data availability—The data that support the findings of this article are openly available [105].

[1] N. G. Van Kampen, *Stochastic Processes in Physics and Chemistry* (Elsevier, New York, 1992), Vol. 1.
[2] J. Preskill, Quantum computing in the NISQ era and beyond, Quantum **2**, 79 (2018).
[3] F. Nogrette, H. Labuhn, S. Ravets, D. Barredo, L. Béguin, A. Vernier, T. Lahaye, and A. Browaeys, Single-atom trapping in holographic 2d arrays of microtraps with arbitrary geometries, Phys. Rev. X **4**, 021034 (2014).
[4] D. Barredo, V. Lienhard, S. De Leseleuc, T. Lahaye, and A. Browaeys, Synthetic three-dimensional atomic structures assembled atom by atom, Nature (London) **561**, 79 (2018).
[5] L. Henriet, L. Beguin, A. Signoles, T. Lahaye, A. Browaeys, G.-O. Reymond, and C. Jurczak, Quantum computing with neutral atoms, Quantum **4**, 327 (2020).
[6] P. Scholl, M. Schuler, H. J. Williams, A. A. Eberharter, D. Barredo, K.-N. Schymik, V. Lienhard, L.-P. Henry, T. C. Lang, T. Lahaye *et al.*, Quantum simulation of 2d antiferromagnets with hundreds of Rydberg atoms, Nature (London) **595**, 233 (2021).
[7] S. Ebadi *et al.*, Quantum optimization of maximum independent set using Rydberg atom arrays, Science **376**, 1209 (2022).
[8] I. Cong, H. Levine, A. Keesling, D. Bluvstein, S.-T. Wang, and M. D. Lukin, Hardware-efficient, fault-tolerant quantum computation with Rydberg atoms, Phys. Rev. X **12**, 021049 (2022).
[9] D. Bluvstein, H. Levine, G. Semeghini, T. T. Wang, S. Ebadi, M. Kalinowski, A. Keesling, N. Maskara, H. Pichler, M. Greiner *et al.*, A quantum processor based on coherent transport of entangled atom arrays, Nature (London) **604**, 451 (2022).

[10] P. Westhoff, S. Paeckel, and M. Moroder, Fast and direct preparation of a genuine lattice Bose-Einstein condensate via the quantum Mpemba effect, Phys. Rev. A **112**, L061304 (2025).
[11] Y. Zhan, Z. Ding, J. Huhn, J. Gray, J. Preskill, G. K.-L. Chan, and L. Lin, Rapid quantum ground state preparation via dissipative dynamics, Phys. Rev. X **16**, 011004 (2026).
[12] G. Teza, F. Campaioli, M. Avesani, and O. Raz, Finite-temperature criticality through quantum annealing, arXiv:2507.07167.
[13] E. B. Mpemba and D. G. Osborne, Cool?, Phys. Educ. **4**, 172 (1969).
[14] G. Teza, J. Bechhoefer, A. Lasanta, O. Raz, and M. Vucelja, Speedups in nonequilibrium thermal relaxation: Mpemba and related effects, Phys. Rep. **1164**, 1 (2026).
[15] Z. Lu and O. Raz, Nonequilibrium thermodynamics of the Markovian Mpemba effect and its inverse, Proc. Natl. Acad. Sci. U.S.A. **114**, 5083 (2017).
[16] I. Klich, O. Raz, O. Hirschberg, and M. Vucelja, Mpemba index and anomalous relaxation, Phys. Rev. X **9**, 021060 (2019).
[17] A. Gal and O. Raz, Precooling strategy allows exponentially faster heating, Phys. Rev. Lett. **124**, 060602 (2020).
[18] R. Yaacoby, O. Raz, and G. Teza, Far from equilibrium relaxation in the weak coupling limit, arXiv:2203.11644.
[19] G. Teza, R. Yaacoby, and O. Raz, Relaxation shortcuts through boundary coupling, Phys. Rev. Lett. **131**, 017101 (2023).
[20] G. Teza, R. Yaacoby, and O. Raz, Eigenvalue crossing as a phase transition in relaxation dynamics, Phys. Rev. Lett. **130**, 207103 (2023).
[21] F. Carollo, A. Lasanta, and I. Lesanovsky, Exponentially accelerated approach to stationarity in Markovian open quantum systems through the Mpemba effect, Phys. Rev. Lett. **127**, 060401 (2021).
[22] T. Mori and T. Shirai, Symmetrized Liouvillian gap in Markovian open quantum systems, Phys. Rev. Lett. **130**, 230404 (2023).
[23] X. Wang and J. Wang, Mpemba effects in nonequilibrium open quantum systems, Phys. Rev. Res. **6**, 033330 (2024).
[24] A. Nava and R. Egger, Mpemba effects in open non-equilibrium quantum systems, Phys. Rev. Lett. **133**, 136302 (2024).
[25] R. Bao and Z. Hou, Accelerating quantum relaxation via temporary reset: A Mpemba-inspired approach, Phys. Rev. Lett. **135**, 150403 (2025).
[26] A. Summer, M. Moroder, L. P. Bettmann, X. Turkeshi, I. Marvian, and J. Goold, A resource theoretical unification of Mpemba effects: Classical and quantum, Phys. Rev. X (2026).
[27] A. Kumar and J. Bechhoefer, Exponentially faster cooling in a colloidal system, Nature (London) **584**, 64 (2020).
[28] A. Kumar, R. Chétrite, and J. Bechhoefer, Anomalous heating in a colloidal system, Proc. Natl. Acad. Sci. U.S.A. **119**, e2118484119 (2022).
[29] M. Ibáñez, C. Dieball, A. Lasanta, A. Godec, and R. A. Rica, Heating and cooling are fundamentally asymmetric and evolve along distinct pathways, Nat. Phys. **20**, 135 (2024).
[30] S. Aharony Shapira, Y. Shapira, J. Markov, G. Teza, N. Akerman, O. Raz, and R. Ozeri, Inverse Mpemba effect demonstrated on a single trapped ion qubit, Phys. Rev. Lett. **133**, 010403 (2024).
[31] J. Zhang, G. Xia, C.-W. Wu, T. Chen, Q. Zhang, Y. Xie, W.-B. Su, W. Wu, C.-W. Qiu, P.-X. Chen *et al.*, Observation of quantum strong Mpemba effect, Nat. Commun. **16**, 301 (2025).
[32] A. Lasanta, F. Vega Reyes, A. Prados, and A. Santos, When the hotter cools more quickly: Mpemba effect in granular fluids, Phys. Rev. Lett. **119**, 148001 (2017).
[33] I. G.-A. Pemartín, E. Mompó, A. Lasanta, V. Martín-Mayor, and J. Salas, Shortcuts of freely relaxing systems using equilibrium physical observables, Phys. Rev. Lett. **132**, 117102 (2024).
[34] A. Lapolla and A. Godec, Faster uphill relaxation in thermodynamically equidistant temperature quenches, Phys. Rev. Lett. **125**, 110602 (2020).
[35] S. Bera, M. R. Walker, and M. Vucelja, Effect of dynamics on anomalous thermal relaxations and information exchange, arXiv:2308.04557.
[36] M. R. Walker, S. Bera, and M. Vucelja, Optimal transport and anomalous thermal relaxations, arXiv:2307.16103.
[37] Á. Tejero, R. Sánchez, L. E. Kaoutit, D. Manzano, and A. Lasanta, Asymmetries of thermal processes in open quantum systems, Phys. Rev. Res. **7**, 023020 (2025).
[38] A. K. Chatterjee, S. Takada, and H. Hayakawa, Quantum Mpemba effect in a quantum dot with reservoirs, Phys. Rev. Lett. **131**, 080402 (2023).
[39] M. Moroder, O. Culhane, K. Zawadzki, and J. Goold, Thermodynamics of the quantum Mpemba effect, Phys. Rev. Lett. **133**, 140404 (2024).
[40] A. Nava and R. Egger, Pontus-Mpemba effects, Phys. Rev. Lett. **135**, 140404 (2025).
[41] F. Ares, S. Murciano, and P. Calabrese, Entanglement asymmetry as a probe of symmetry breaking, Nat. Commun. **14**, 2036 (2023).
[42] C. Rylands, K. Klobas, F. Ares, P. Calabrese, S. Murciano, and B. Bertini, Microscopic origin of the quantum Mpemba effect in integrable systems, Phys. Rev. Lett. **133**, 010401 (2024).
[43] F. Ares, P. Calabrese, and S. Murciano, The quantum Mpemba effects, Nat. Rev. Phys. **7**, 451 (2025).
[44] R. Bao, companion Letter, Initial-state typicality in quantum relaxation, Phys. Rev. Lett. **136**, 070402 (2026).
[45] B. Buča and T. Prosen, A note on symmetry reductions of the Lindblad equation: Transport in constrained open spin chains, New J. Phys. **14**, 073007 (2012).
[46] V. V. Albert, B. Bradlyn, M. Fraas, and L. Jiang, Geometry and response of Lindbladians, Phys. Rev. X **6**, 041031 (2016).
[47] D. Manzano and P. Hurtado, Harnessing symmetry to control quantum transport, Adv. Phys. **67**, 1 (2018).
[48] J. Dubois, U. Saalmann, and J. M. Rost, Symmetry-induced decoherence-free subspaces, Phys. Rev. Res. **5**, L012003 (2023).
[49] M. Boneberg, F. Carollo, and I. Lesanovsky, Nonlinear classification capability of quantum neural networks due to emergent quantum metastability, Phys. Rev. A **111**, 062405 (2025).
[50] V. Gorini, A. Kossakowski, and E. C. G. Sudarshan, Completely positive dynamical semigroups of n-level systems, J. Math. Phys. (N.Y.) **17**, 821 (1976).

[51] G. Lindblad, On the generators of quantum dynamical semigroups, Commun. Math. Phys. **48**, 119 (1976).

[52] B. Baumgartner and H. Narnhofer, Analysis of quantum semigroups with GKS–Lindblad generators: II. General, J. Phys. A **41**, 395303 (2008).

[53] T. Prosen, Spectral theorem for the Lindblad equation for quadratic open fermionic systems, J. Stat. Mech. (2010) P07020.

[54] F. Benatti and R. Floreanini, Open quantum dynamics: Complete positivity and entanglement, Int. J. Mod. Phys. B **19**, 3063 (2005).

[55] D. Manzano, A short introduction to the Lindblad master equation, AIP Adv. **10**, 025106 (2020).

[56] H. Breuer and F. Petruccione, *The Theory of Open Quantum Systems* (Oxford University Press, New York, 2002).

[57] R. Alicki and K. Lendi, *Quantum Dynamical Semigroups and Applications*, Vol. 717 (Springer, New York, 2007).

[58] C. Gardiner and P. Zoller, *Quantum Noise: A Handbook of Markovian and Non-Markovian Quantum Stochastic Methods with Applications to Quantum Optics*, Springer Series in Synergetics (Springer, New York, 2004).

[59] A. Rivas and S. F. Huelga, *Open Quantum Systems: An Introduction* (Springer, Berlin, Heidelberg, 2012).

[60] R. Fazio, J. Keeling, L. Mazza, and M. Schirò, Many-body open quantum systems, arXiv:2409.10300.

[61] Here, $\mathcal{L}^\dagger$ is the adjoint Lindblad map defined by $\mathrm{Tr}(\rho_1^\dagger \mathcal{L}[\rho_2]) = \mathrm{Tr}(\mathcal{L}^\dagger[\rho_1^\dagger]\rho_2)$, for arbitrary density matrices ρ_1, ρ_2.

[62] V. V. Albert, Lindbladians with multiple steady states: Theory and applications, arXiv:1802.00010.

[63] See Supplemental Material at http://link.aps.org/supplemental/10.1103/4frd-ck2z for additional details of the calculations at the basis of the results presented in the main text.

[64] L. Kohaupt, Introduction to a gram-schmidt-type biorthogonalization method, Rocky Mt. J. Math. **44**, 1265 (2014).

[65] D. E. Evans and H. Hanche-Olsen, The generators of positive semigroups, J. Funct. Anal. **32**, 207 (1979).

[66] D. E. Evans, Irreducible quantum dynamical semigroups, Commun. Math. Phys. **54**, 293 (1977).

[67] D. Manzano and P. I. Hurtado, Symmetry and the thermodynamics of currents in open quantum systems, Phys. Rev. B **90**, 125138 (2014).

[68] V. V. Albert and L. Jiang, Symmetries and conserved quantities in Lindblad master equations, Phys. Rev. A **89**, 022118 (2014).

[69] A. Frigerio, Stationary states of quantum dynamical semigroups, Commun. Math. Phys. **63**, 269 (1978).

[70] A. M. van den Brink and K. Young, Jordan blocks and generalized bi-orthogonal bases: Realizations in open wave systems, J. Phys. A **34**, 2607 (2001).

[71] Z. Zhang, J. Tindall, J. Mur-Petit, D. Jaksch, and B. Buča, Stationary state degeneracy of open quantum systems with non-Abelian symmetries, J. Phys. A **53**, 215304 (2020).

[72] J. Thingna and D. Manzano, Degenerated Liouvillians and steady-state reduced density matrices, Chaos **31**, 073114 (2021).

[73] The full diagonalization of the Liouvillian is *not* required; it is sufficient to identify the (slow or fast) eigenmodes to be suppressed. Our discussion can be generalized to nondiagonalizable Liouvillians, mappable into Jordan canonical form; however, the recipe we present will not apply to Liouvillian modes in nondiagonalizable blocks.

[74] More formally, $\ell_a^\dagger \in \mathcal{A}$, $\forall\ \ell_a \in \mathcal{A}$. This forbids the inclusion in $\mathcal{A}$ of a single element from a pair of Hermitian-conjugated left eigenmatrices, $\{\ell_i, \ell_{i+1}\}$, $\ell_i = \ell_{i+1}^\dagger$.

[75] In the case of a pure initial state, $\rho_0 = |\psi_0\rangle\langle\psi_0|$, it is sufficient to compute the eigenvector of $\bar{\rho}_\perp$ associated with the largest eigenvalue; the full diagonalization of $\bar{\rho}_\perp$ is not necessary.

[76] F. Campaioli, W. Sloan, K. Modi, and F. A. Pollock, Algorithm for solving unconstrained unitary quantum brachistochrone problems, Phys. Rev. A **100**, 062328 (2019).

[77] C. P. Koch, U. Boscain, T. Calarco, G. Dirr, S. Filipp, S. J. Glaser, R. Kosloff, S. Montangero, T. Schulte-Herbrüggen, D. Sugny *et al.*, Quantum optimal control in quantum technologies. Strategic report on current status, visions and goals for research in europe, Eur. Phys. J. Quantum Technol. **9**, 19 (2022).

[78] Q. Ansel, E. Dionis, F. Arrouas, B. Peaudecerf, S. Guérin, D. Guéry-Odelin, and D. Sugny, Introduction to theoretical and experimental aspects of quantum optimal control, J. Phys. B **57**, 133001 (2024).

[79] D. d'Alessandro, *Introduction to Quantum Control and Dynamics*, 2nd ed. (Chapman and Hall/CRC, London, 2021).

[80] D. Lewis, R. Wiersema, J. Carrasquilla, and S. Bose, Geodesic algorithm for unitary gate design with time-independent Hamiltonians, Phys. Rev. A **111**, 052618 (2025).

[81] J. Johansson, P. Nation, and F. Nori, QuTiP 2: A Python framework for the dynamics of open quantum systems, Comput. Phys. Commun. **184**, 1234 (2013).

[82] In Fig. 3, we neglect T_U as it depends on the quantum hardware (types of gates available, duration of their execution, etc.).

[83] M. Bukov, D. Sels, and A. Polkovnikov, Geometric speed limit of accessible many-body state preparation, Phys. Rev. X **9**, 011034 (2019).

[84] S. Kochsiek, F. Carollo, and I. Lesanovsky, Accelerating the approach of dissipative quantum spin systems towards stationarity through global spin rotations, Phys. Rev. A **106**, 012207 (2022).

[85] L. Henriet, L. Beguin, A. Signoles, T. Lahaye, A. Browaeys, G.-O. Reymond, and C. Jurczak, Quantum computing with neutral atoms, Quantum **4**, 327 (2020).

[86] R. B.-S. Tsai, H. Silvério, and L. Henriet, Pulse-level scheduling of quantum circuits for neutral-atom devices, Phys. Rev. Appl. **18**, 064035 (2022).

[87] D. Bluvstein, H. Levine, G. Semeghini, T. T. Wang, S. Ebadi, M. Kalinowski, A. Keesling, N. Maskara, H. Pichler, M. Greiner *et al.*, A quantum processor based on coherent transport of entangled atom arrays, Nature (London) **604**, 451 (2022).

[88] The choice of the ansatz depends on the specific problem. Even though more sophisticated gates can also be considered, the ansatz should be kept as simple as possible to minimize the preparation time, T_U, and simplify the optimization procedure.

[89] G. Pichard, D. Lim, E. Bloch, J. Vaneecloo, L. Bourachot, G.-J. Both, G. Mériaux, S. Dutartre, R. Hostein, J. Paris,

B. Ximenez, A. Signoles, A. Browaeys, T. Lahaye, and D. Dreon, Rearrangement of individual atoms in a 2000-site optical-tweezer array at cryogenic temperatures, Phys. Rev. Appl. **22**, 024073 (2024).
[90] S. de Léséleuc, D. Barredo, V. Lienhard, A. Browaeys, and T. Lahaye, Analysis of imperfections in the coherent optical excitation of single atoms to Rydberg states, Phys. Rev. A **97**, 053803 (2018).
[91] J. Dubois, U. Saalmann, and J. M. Rost, Semi-classical Lindblad master equation for spin dynamics, J. Phys. A **54**, 235201 (2021).
[92] S. Dutta, S. Zhang, and M. Haque, Quantum origin of limit cycles, fixed points, and critical slowing down, Phys. Rev. Lett. **134**, 050407 (2025).
[93] G. Villa, J. del Pino, V. Dumont, G. Rastelli, M. Michałek, A. Eichler, and O. Zilberberg, Topological classification of driven-dissipative nonlinear systems, Sci. Adv. **11**, eadt9311 (2025).
[94] L. Carde, R. Gautier, N. Didier, A. Petrescu, J. Cohen, and A. McDonald, Non-perturbative switching rates in bistable open quantum systems: From driven Kerr oscillators to dissipative cat qubits, arXiv:2507.18714.
[95] T. Banerjee, S. Choudhury, and K. Sengupta, Exact floquet flat band and heating suppression via two-rate drive protocols, New J. Phys. **27**, 084506 (2025).
[96] A. Quarteroni, R. Sacco, and F. Saleri, *Numerical Mathematics* (Springer, New York, 2007).
[97] C. G. Broyden, A class of methods for solving nonlinear simultaneous equations, Math. Comput. **19**, 577 (1965).
[98] D. G. Anderson, Iterative procedures for nonlinear integral equations, J. ACM **12**, 547 (1965).
[99] M. S. Byrd and N. Khaneja, Characterization of the positivity of the density matrix in terms of the coherence vector representation, Phys. Rev. A **68**, 062322 (2003).
[100] G. Kimura, The Bloch vector for n-level systems, Phys. Lett. A **314**, 339 (2003).
[101] S. U. Chung and T. L. Trueman, Positivity conditions on the spin density matrix: A simple parametrization, Phys. Rev. D **11**, 633 (1975).
[102] S. M. Deen, P. K. Kabir, and G. Karl, Positivity constraints on density matrices, Phys. Rev. D **4**, 1662 (1971).
[103] I. Bengtsson, S. Weis, and K. Życzkowski, Geometry of the set of mixed quantum states: An apophatic approach, in *Geometric Methods in Physics* (Springer, Basel, 2013), pp. 175–197.
[104] D. Gamarnik, C. Moore, and L. Zdeborová, Disordered systems insights on computational hardness, J. Stat. Mech. (2022) P114015.
[105] N. Beato and G. Teza, Relaxation control of open quantum systems, Zenodo, 10.5281/zenodo.18198689 (2026).

End Matter

Slowdown of the relaxation dynamics—Here, we demonstrate an alternative application of the recipe introduced in the main text, illustrating how the method can also be employed to slow down the relaxation dynamics. Here, we use the recipe to selectively suppress the projection of the initial density matrix ρ_0 along all except the slowest decaying mode(s).

In Fig. 4, we demonstrate the slowdown of the relaxation dynamics toward the steady state in the open quantum Ising chain defined in Eqs. (9) and (10). This is achieved by reducing the projection of the initial state ρ_0 onto all except the slowest Liouvillian decaying mode(s), $\mathcal{A}_{\parallel} = \{\ell_a\}_{a>2}$ (or $\mathcal{A}_{\parallel} = \{\ell_a\}_{a>3}$, in case $\lambda_2 = \lambda_3^*$). The figure shows the trajectories of the original initial state $\rho_0(t)$ (black curve), the state generated by the recipe $\rho_{\parallel}(t)$ (solid red), and the experimentally accessible unitary $\check{\rho}_{\parallel}(t)$ [dashed red; cf. Eq. (13)].

To achieve a significant slowdown in the relaxation dynamics, the tolerance for the algorithm's convergence can be set smaller compared to the speedup case, e.g., $\epsilon \sim 10^{-1}$. For a quantitative comparison, in the case of relaxation speedup, we set $\epsilon = 10^{-6}$ [63]. From Fig. 4, we see that the relatively smaller tolerance allows a considerable slowdown of the relaxation process. In particular, we observe that the distance between the transformed state $\rho_{\parallel}$ and the steady state ρ_∞ is almost one order of magnitude

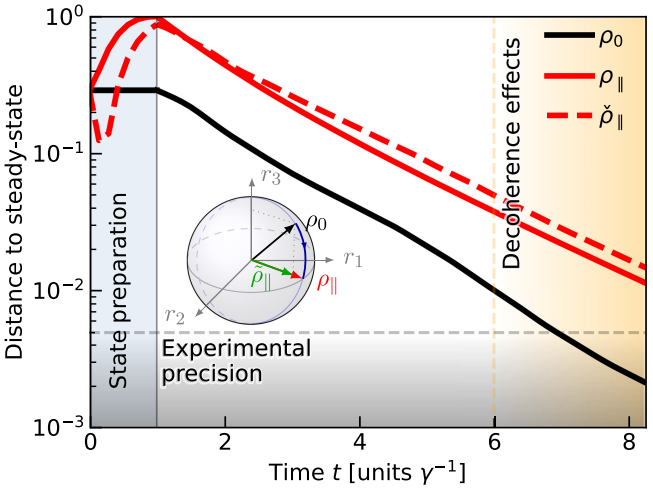


FIG. 4. Slowdown of the relaxation dynamics toward the steady state in the open quantum Ising chain in Eqs. (9) and (10) ($N = 5, h_x = 1, J = 1.25, \alpha = 0.5$, and $\gamma = 1$). We use the recipe introduced in the main text to selectively suppress the projection of the initial density matrix ρ_0 along all except the slowest-decaying mode. The plot shows the distance to the steady state ρ_∞ of the initial and transformed states $\rho_0(t), \rho_{\parallel}(t), \check{\rho}_{\parallel}(t)$ (black, solid-red, and dashed-red curves, respectively). The dashed line refers to the state preparation obtained with the single-qubit transformation in Eq. (13). This result demonstrates the efficacy of the recipe for the slowdown of the relaxation dynamics.

larger, as compared to the initial state ρ_0. Lastly, we notice that the state prepared with the experimentally accessible unitary operation exhibits a relaxation trajectory (dashed red) qualitatively close to the theoretical unitary transformation (solid red).

These results show how the recipe introduced in the main text can also be applied to extend the relaxation dynamics of the open quantum system.